Crustal structure and origin of the Eggvin Bank west of Jan Mayen, NE Atlantic

Correspondence to:
P. Tan,
pingchuan.tan@geo.uio.no

Pingchuan Tan[1] , **Asbjørn Johan Breivik[1]** , **Reidar G. Trønnes[2]** , **Rolf Mjelde[3]** , **Ryosuke Azuma[4, 5]** , **and Sigurd Eide[6,7]**

[1]Centre for Earth Evolution and Dynamics, Department of Geosciences, University of Oslo, Oslo, Norway, [2]Centre for Earth Evolution and Dynamics, and Natural History Museum, University of Oslo, Oslo, Norway, [3]Department of Earth Science, University of Bergen, Bergen, Norway, [4]Institute of Seismology and Volcanology, Faculty of Science, Hokkaido University, Sapporo, Japan, [5]Now at Research Center for Prediction of Earthquake and Volcanic Eruption, Graduation School of Science, Tohoku University, Sendi, Japan, [6]Navigeo, Oslo, Norway, [7]First Geo, Oslo, Norway

Abstract The Eggvin Bank, located between the Jan Mayen Island and Greenland, is an unusually shallow area containing several submarine volcanic peaks, confined by two transforms on the Northern Kolbeinsey Ridge (NKR). We represent *P* and *S* wave velocity models for the Eggvin Bank based on an Ocean Bottom Seismometer profile collected in 2011, showing igneous crustal thickness variations from 8 km to 13 km. A 2–5 km increase is associated with two separate 20–30 km wide segments under the main seamounts. The oceanic crust has three layers: upper crust (L2A: 2.8–4.8 km/s), middle crust (L2B: 5.5–6.5 km/s), and lower crust (L3: 6.7–7.35 km/s). Both the thick layer 2(A/B) and the high ratio of layer 2(A/B) thickness to total crustal thickness indicate that secondary, intraplate magmatism built the seamounts of the Eggvin Bank. The seamount in the north where the crust is thickest has a flat top indicating subaerial exposure but is deeper than those with rounded tops in the south and is therefore probably older. Comparing lower crustal seismic velocity with crustal thickness also indicates that the degree of mantle melting may be higher in the north than in the south. An enriched mantle source presently feeds the NKR magmatism and probably influenced the Eggvin Bank development also at earlier times. To what extent the Eggvin Bank has been influenced by the Iceland plume is uncertain, both an enriched mantle component and elevated mantle temperature may have played a role at different times and locations.

1. Introduction

The impingement of the Iceland plume head caused extensive magmatism in the Northeast Atlantic during Paleocene-Early Eocene. During the first few million years after continental breakup volcanic margins characterized by thickened oceanic crust were created. After that, most excess volcanism occurred along the Faeroe-Iceland-Greenland ridge [e.g., *Eldholm and Grue*, 1994]. Today, the Norwegian island of Jan Mayen has an active volcano, and recent research [*Kandilarov et al.*, 2012, 2015] has increasingly highlighted the surrounding areas affected by postbreakup magmatic processes (Figure 1). The Eggvin Bank is located between Jan Mayen and the east coast of Greenland, straddling the axial zone of the Northern Kolbeinsey Ridge (NKR). It is an unusually shallow area, containing several submarine volcanic peaks as well as large central volcanic edifices as shallow as 30 m below sea level [*Haase et al.*, 2003]. The southern margin of the Eggvin Bank coincides with a small offset on the Kolbeinsey Ridge, whereas the northern boundary is the West Jan Mayen Fracture Zone(WJMFZ), partly a large transform fault between the Kolbeinsey and Mohn's ridges (Figure 2). The NKR has a slow half-spreading rate of 9 mm/yr [*Mosar et al.*, 2002; *Gaina et al.*, 2009]. Compared with the middle Kolbeinsey Ridge (MKR), the magmatism at NKR including the Eggvin Bank is enriched in incompatible elements and radiogenic isotopic compositions [e.g., *Campsie et al.*, 1990; *Haase et al.*, 2003; *Mertz et al.*, 2004; *Elkins et al.*, 2011, 2016]. The asymmetric bathymetry across the spreading axis, as well as indistinct magnetic lineations on the Eggvin Bank [*Maus et al.*, 2007], may indicate a significant off-axis magmatic activity. The majority of the seamounts are located between NKR and Jan Mayen. Large volcanic edifices with high magma supply straddle the spreading axis [*Yeo et al.*, 2012; *Elkins et al.*, 2013; *Yeo et al.*, 2016]. The development of the Eggvin Bank is affected by the proximity to the Kolbeinsey
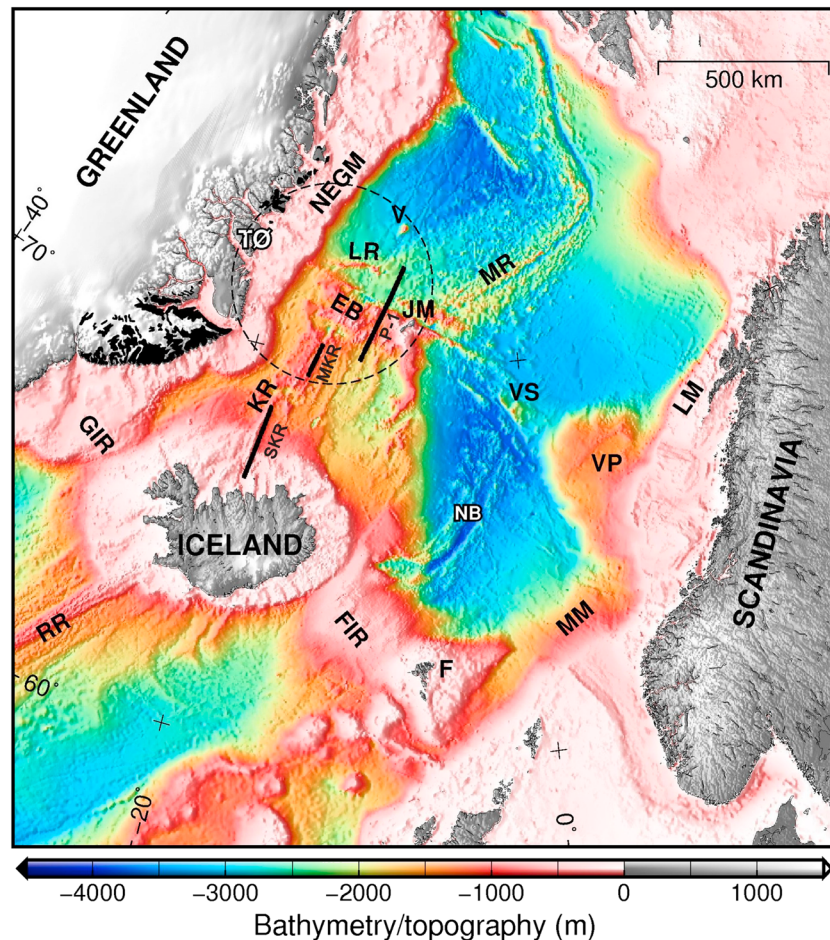
Figure 1. Bathymetry map (ETOPO2v2) [*U.S. Department of Commerce et al.*, 2006] showing regional features, where the study area (Figure 2) is indicated by the dashed circle, and the studied profile is marked P-1 (Profile-1). The position of older OBS profiles by *Kodaira et al.* [1997] (MKR) and *Hooft et al.* [2006] (SKR) is also shown. Early Cenozoic basalt flows or intrusions are illustrated as black areas onshore Greenland [*Noble et al.*, 1988]. EB: Eggvin Bank, F: Faeroes, FIR: Faeroes-Iceland Ridge, GIR: Greenland-Iceland Ridge, JM: Jan Mayen, KR: Kolbeinsey Ridge, LM: Lofoten Margin, LR: Logi Ridge, MKR: Middle Kolbeinsey Ridge, MM: Møre Margin, MR: Mohn's Ridge, NB: Norway Basin, NEGM: Northeast Greenland Margin, RR: Reykjanes Ridge, SKR: South Kolbeinsey Ridge, TØ: Traill Ø, VP: Vøring Plateau, VS: Vøring Spur, and V: Vesteris Seamount.

and Mohn's spreading ridges, the Jan Mayen microcontinent (JMMC), and the active WJMFZ [*Yeo et al.*, 2012; *Elkins et al.*, 2013].

The JMMC separated from east Greenland at about 24 Ma [*Talwani and Eldholm*, 1977; *Vogt et al.*, 1980; *Gaina et al.*, 2009] (Figure 2). The continent-ocean transition (COT) along the JMMC margins was constrained by *Peron-Pinvidic et al.* [2012a, 2012b] mainly based on seismic reflection data combined with magnetic and gravity data. Wide-angle seismic data further constrains the northern boundary of the JMMC which coincides with the continuation of the northern lineament of the East Jan Mayen Fracture Zone (EJMFZ) [*Kandilarov et al.*, 2012]. Eastern and western boundaries have been defined by *Breivik et al.* [2012] and *Kodaira et al.* [1998a], respectively (Figure 2).

Based on early refraction data, *Sørnes and Navrestad* [1975] concluded that the crustal thickness in the Jan Mayen and Eggvin Bank area is around 16 km, while *Evans and Sacks* [1979] suggested that the crustal thickness is about 20 km based on the study of earthquakes along the WJMFZ. Two regional 3-D crustal models of the NE Atlantic have recently been published. *Funck et al.* [2016] indicate a crustal thickness of 6–8 km in the Eggvin Bank but lack seismic constraints there. With the added control of gravity using inversion, *Haase et al.* [2016] found a crustal thickness of 10–15 km. Other seismic refraction surveys document surrounding areas: the oceanic crustal thickness in the Greenland basin is around 4–5 km [*Klingelhöfer et al.*, 2000; *Voss and*
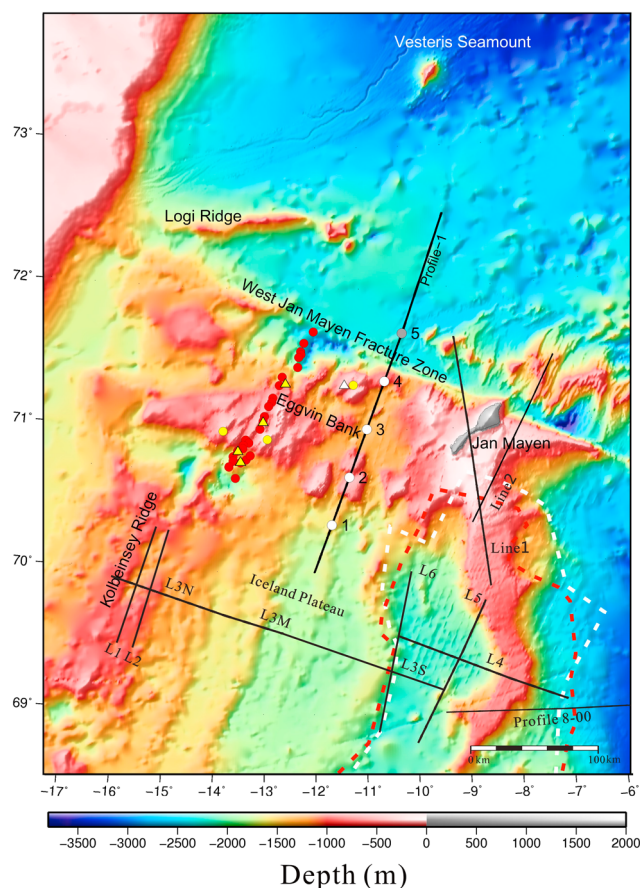
Figure 2. Layout of the survey shown on IBCAO (v.3) bathymetry [*Jakobsson et al.*, 2012]. Profile-1 is the OBS profile, where circles show OBS positions, and white fill indicates useful data. Several previous OBS based crustal studies around Eggvin Bank are shown (Jan Mayen microcontinent (L3S, L4, L5, L6), Kolbeinsey Ridge (L1, L2, L3N), Iceland Plateau (L3M) [*Kodaira et al.*, 1997, 1998a, 1998b], southern part of the Jan Mayen microcontinent (Profiles 8–00) [*Breivik et al.*, 2012], and northern part of the Jan Mayen microcontinent (Line 1 and Line 2) [*Kandilarov et al.*, 2012]). The north part of the Kolbeinsey ridge (NKR) has been investigated geochemically from dredged samples (red circles [*Haase et al.*, 2003], yellow circles [*Mertz et al.*, 2004], yellow triangles [*Elkins et al.*, 2011], and white triangles [*Campsie et al.*, 1990]). The white dashed line represents the location of the continental ocean boundary (COB) around the JMMC by *Breivik et al.* [2012] incorporating results from *Kandilarov et al.* [2012], while the red dashed line shows the COB by *Peron-Pinvidic et al.* [2012a, 2012b].

Jokat, 2007; *Voss et al.*, 2009; *Kandilarov et al.*, 2012]; the northern Iceland plateau has a larger crustal thickness around 9.5 km [*Kodaira et al.*, 1998b; 2002; 2007]; the continental crustal thickness is more than 25 km at the northern boundary of the JMMC, while the oceanic crustal thickness north of the Jan Mayen island across the WJMFZ is up to 12 km [*Kandilarov et al.*, 2012].

The origin of the Eggvin Bank has been the subject of debate. Based on the early seismic studies and the geochemical analysis of dredged samples from the Eggvin Bank, *Campsie et al.* [1990] suggested that the thickened Eggvin Bank could be due to underlying continental crust extending from JMMC. Some authors have ascribed the Jan Mayen and Eggvin Bank volcanism to a mantle plume around Jan Mayen [e.g., *Schilling et al.*, 1983; *Elkins et al.*, 2016], and *Morgan* [1983] suggested that the Eggvin Bank could be a hot spot track. Several geochemical studies, however, suggest a likely connection with the lateral flow of Iceland plume material [e.g., *Trønnes et al.*, 1999; *Mertz et al.*, 2004]. The V-shaped ridges along the Kolbeinsey spreading axis also indicate that the lateral flow of pulses from the Iceland plume extends all the way to the WJMFZ [*Jones et al.*, 2002]. The Jan Mayen and Eggvin Bank volcanism has also been related to minor spreading or leakage along WJFMZ [*Imsland*, 1986; *Havskov and Atakan*, 1991; *Gernigon et al.*, 2008; *Kandilarov et al.*, 2012]. However, most of the magmatism is located to the south of the active transform, suggesting that this is not an important mechanism.
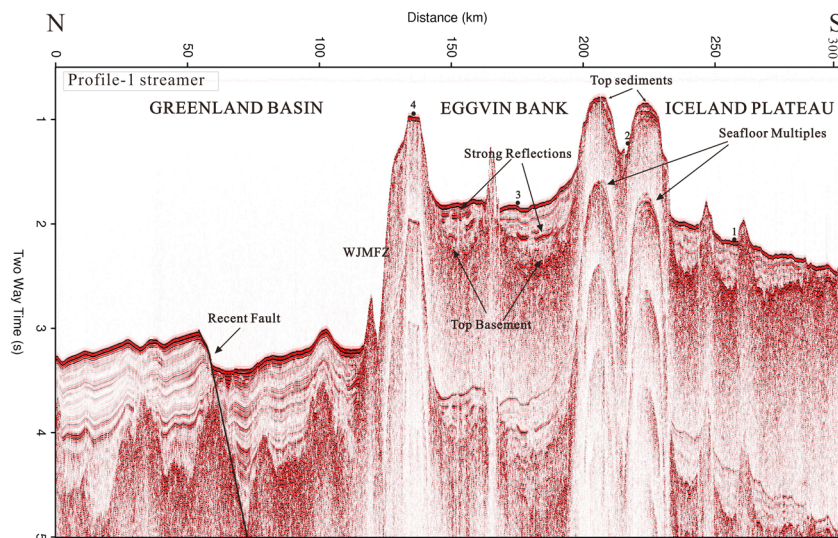
Figure 3. Single-channel streamer reflection seismic data of Profile-1. OBS locations are illustrated with black circles, with the instrument number above. WJFMZ: West Jan Mayen Fracture Zone.

In this study, we use wide-angle seismic data in order to constrain the crustal velocity structure in detail along a single transect over the Eggvin Bank. This will be used to discuss the distribution of excess magmatism, process that can cause it, and to roughly address possible differences in timing of magmatic events along profile.

2. Data Acquisition and Processing

This marine geophysical survey was conducted between Jan Mayen and East Greenland during early fall of 2011 by the R/V *Håkon Mosby*. It is a collaboration between the Department of Geoscience, University of Oslo, Department of Earth Science, University of Bergen, and the Institute of Seismology and Volcanology, Hokkaido University, Sapporo, Japan. The seismic source consisted of four equal-sized Bolt air guns with a total volume of 78.6 L, which were fired every 200 m. The ocean bottom seismometers (OBS) were deployed approximately N-S from the Greenland Basin across the Eggvin Bank (Figure 2). Four OBSs returned good data sets, while OBS 5 in the north failed. Each OBS is composed of 4.5 Hz three-component geophones. The air gun signals were recorded by a digital audio tape recorder with a 16 bit analog to digital converter sampling at 256 Hz. A single-channel streamer was also used to record near-vertical seismic reflection data.

The OBS preprocessing consisted of extracting a 60 s record length of each shot, OBS position adjustment and linking to navigation. The OBS data processing consisted of 8 km/s or 4.6 km/s velocity reduction for *P* and *S* wave data respectively, 5–12 Hz band-pass filtering, offset-dependent amplitude scaling or automatic gain control (2 s window), and spiking deconvolution. The sea-floor depth was obtained from echo sounder recordings on board the ship. The single channel streamer profile was processed with spiking deconvolution, 5–60 Hz band-pass filter and amplitude corrections with a geometrical exponential factor of 1.2. It produced good-quality reflection seismic data, which was used to constrain sedimentary thickness for the starting velocity model (Figure 3). Using a water velocity of 1480 m/s gave a good fit between the seafloor depth observed from echo sounder recordings and the seabed in the seismic profile.

3. Geological Setting

The sediments at the Eggvin Bank and in the surrounding areas consist of mud and silt with some additional ice-drafted materials deposited during the last glacial periods [e.g., *Haase et al.*, 2003; *Thiede and Hempel*, 1991]. A thick sedimentary sequence is observed in the Greenland Basin. The oceanic crust north of the WJMFZ dates from chrons C6 and C7 [*Maus et al.*, 2007; *Engen et al.*, 2008], which indicates that all sediments deposited along profile in the Greenland Basin are younger than 25 Ma. A normal fault offsetting sedimentary strata observed in the Greenland Basin indicates recent tectonic activity north of the Eggvin Bank. Three large seamounts are observed along the Eggvin Bank profile with two of them having thin sedimentary units on

top (Figure 3). The northern seamount is almost sediment free and has a flat top, indicating that it has been eroded above or near the sea surface. At a half-spreading rate of 9 mm/yr, the age would be around 7 Ma in the northern Eggvin Bank, increasing to around 10–11 Ma in the southern Eggvin Bank at the profile position. The sedimentary layers between the southern and northern seamounts have some strong discontinuous reflective layers, which could be interpreted as basaltic intrusions or flows. The upper sedimentary layers on the Eggvin Bank are inclined and follow the slopes of the surrounding peaks, while the sedimentary package on the Iceland Plateau, which has crust around 13.5 Ma old along the profile [*Maus et al.*, 2007; *Engen et al.*, 2008], decreases in thickness toward the south.

4. Velocity Modeling

4.1. *P* Wave Modeling

The 2-D velocity modeling was done with Rayinvr forward/inverse ray tracing software developed by *Zelt and Ellis* [1988, 1992]. The model is processed layer by layer from top water layer to bottom mantle layer by fitting traveltimes with increasing offsets. The model is built on a limited number of velocity and depth nodes. The thickness and velocity of the sedimentary package was calculated by an empirical velocity-depth trend ($V_p = 1.8 + 0.7Z$ km/s, Z: depth in km) based on nearby crustal studies [*Kodaira et al.*, 1997; *Voss et al.*, 2009; *Breivik et al.*, 2012; *Kandilarov et al.*, 2012]. The bathymetry and top basement derived from the echo sound recordings and single-channel streamer reflection seismic line, respectively, are modeled with denser depth nodes. The misfit between the interpreted and modeled traveltimes is estimated by using χ^2 analysis. The χ^2 value evaluates the goodness of fit by the given uncertainty of the interpretation, and a value of 1 or lower per phase represents a fit [*Zelt and Smith*, 1992]. The main uncertainties are arrival time picking, instrument location, shot timing and the bathymetry [*Hooft et al.*, 2000; *Ljones et al.*, 2004]. Minor relocations of some OBSs had to be made (OBS1: 19 m shallower, OBS2: 14 m shallower, OBS3: 12 m shallower). Location uncertainties of up to a few tens of meters would affect travel times by 10–20 ms with typical upper basement/sediment velocities. In this study, we have manually picked a total of 479 refractions and 101 reflection picks. Each pick of arriving phase is assigned an uncertainty in time. It is often assigned to a typical cycle width of the phase [*Breivik et al.*, 2003]. The uncertainties of the short offset arrivals from sedimentary layers, and upper and middle parts of crust (P_{g1} and P_{g2}), which are usually clear and marked by higher frequency than later arrivals, are estimated to ± 50 ms, while the lower part of crust (P_{g3}) and Moho arrivals ($P_M P$ and P_n) are assigned uncertainties of ± 75 ms and ± 100 ms, respectively. The arrivals from most layers (except P_{g1}) have a fit with χ^2 less than 1 (Table 1). The ray tracing and traveltime fit of OBSs 1, 2, 3, and 4 are illustrated in Figures 4–7 and the velocity model in Figure 8.

Poor seismic coverage of the Greenland Basin gives limited information about the crust there, while most parts of the Eggvin Bank and the Iceland Plateau to the south (135–280 km) are better covered. The crust was modeled using of three layers, a lower velocity upper crust (2.8 km/s–4.8 km/s), middle crust (5.5 km/s–6.5 km/s), and a high-velocity, low-gradient lower crustal layer (6.7 km/s–7.35 km/s). Compared to the average oceanic crust [*White et al.*, 1992; *Christeson et al.*, 1994], the velocities of upper crust, middle crust, and lower crust are within the range of the oceanic layer 2A, layer 2B, and layer 3, respectively. Layer 2A is extrusive and consists of pillow lavas, layer 2B corresponds to sheeted dikes, and layer 3 corresponds to gabbros [*Detrick et al.*, 1994; *Dilek*, 1998]. The upper layer (layer 2A), including the seamounts and the uppermost crystalline crust, is well constrained by the P_{g1} and P_{g2} phases. The thickness of 2A is about 1–1.5 km thick in the Iceland Plateau but increase to about 2.5 km in the seamounts of the Eggvin Bank. The basement velocity of the seamounts are below 3.15 km/s, which is lower than the 3.5–3.8 km/s velocity found in the Iceland Plateau to the south. There are only indirect constraints on the upper crustal velocity north of the WJMFZ, where the P_n arrival times are modulated by the top basement topography, indicating similar velocities as to the south of the Eggvin Bank. The middle crust (layer 2B) is well constrained by the refracted arrivals. It is thicker at the Eggvin bank (average 2.5 km) than at the Iceland Plateau (average 1 km). The oceanic layer 2 (upper and middle crustal layer) thickness is quite uniform (4.2 ± 0.5 km) along the Eggvin Bank regardless of the total crustal thickness. Therefore, crustal thickening is mainly resulting from lower crustal variations. There are two crustal roots with quite different Moho depths. The northern (135 km–190 km) has a maximum crustal thickness around 13 km and is constrained by upper mantle refractions (P_n) of OBSs 2–4. The crustal thickness in the

Table 1. Seismic Model Fit Statistics for Individual Major Phases (*P* Wave) and Summary For All Phases

Phase	No. of rays	RMS Δt (ms)	χ^2
Water	60	41	0.689
P_{g1}	42	50	1.029
P_{g2}	39	40	0.518
P_{g3}	259	66	0.777
P_n	139	78	0.615
$P_M P$	41	72	0.534
All phases	580	65	0.707
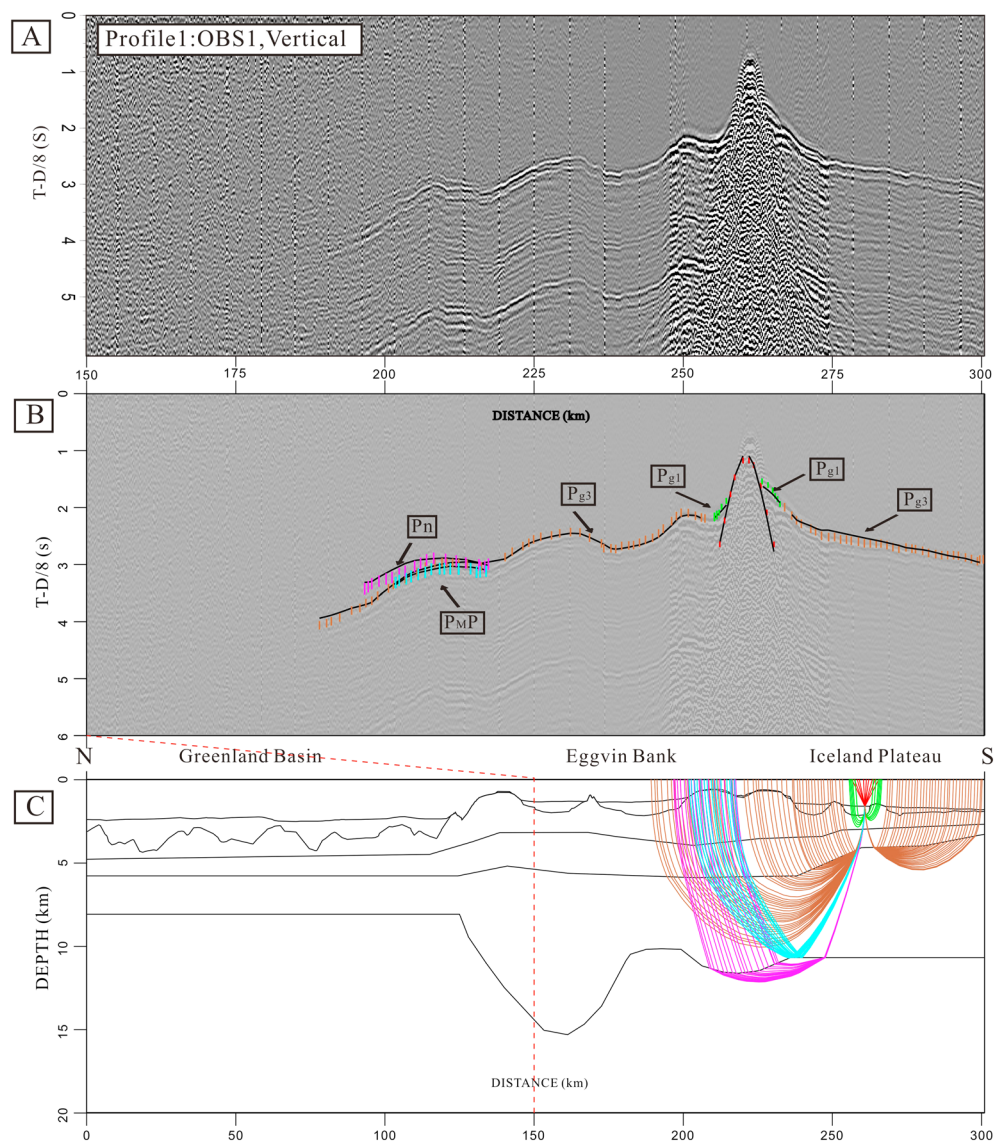
Figure 4. Data, interpretation, and ray tracing of OBS1. (a) Vertical component data of OBS1 reduced by 8 km/s (5–12 Hz band-pass filtered and offset-dependent scaling). (b) Comparison between calculated (black solid line) and interpreted traveltime (colored vertical bars) for OBS1 with data in the background. (c) Ray tracing of the velocity model.
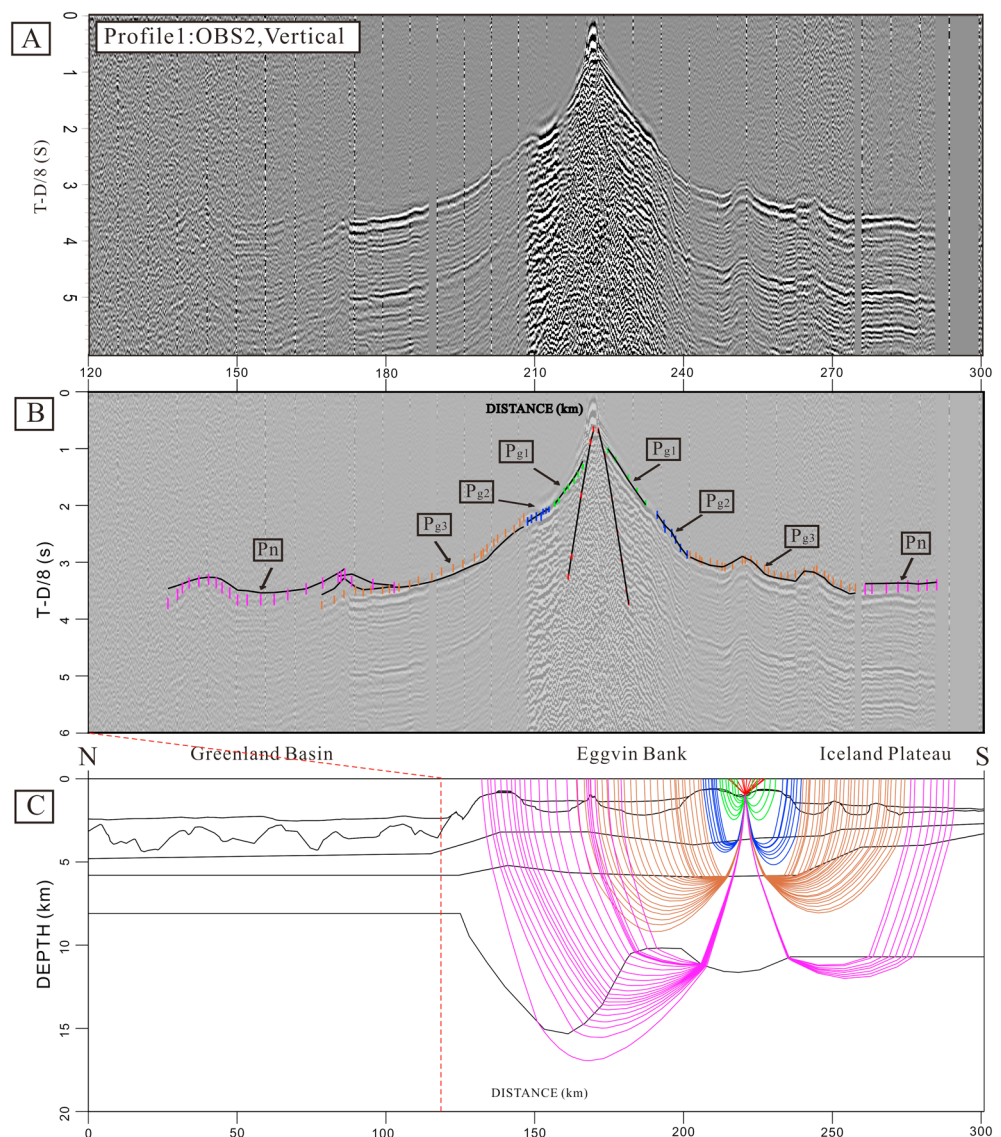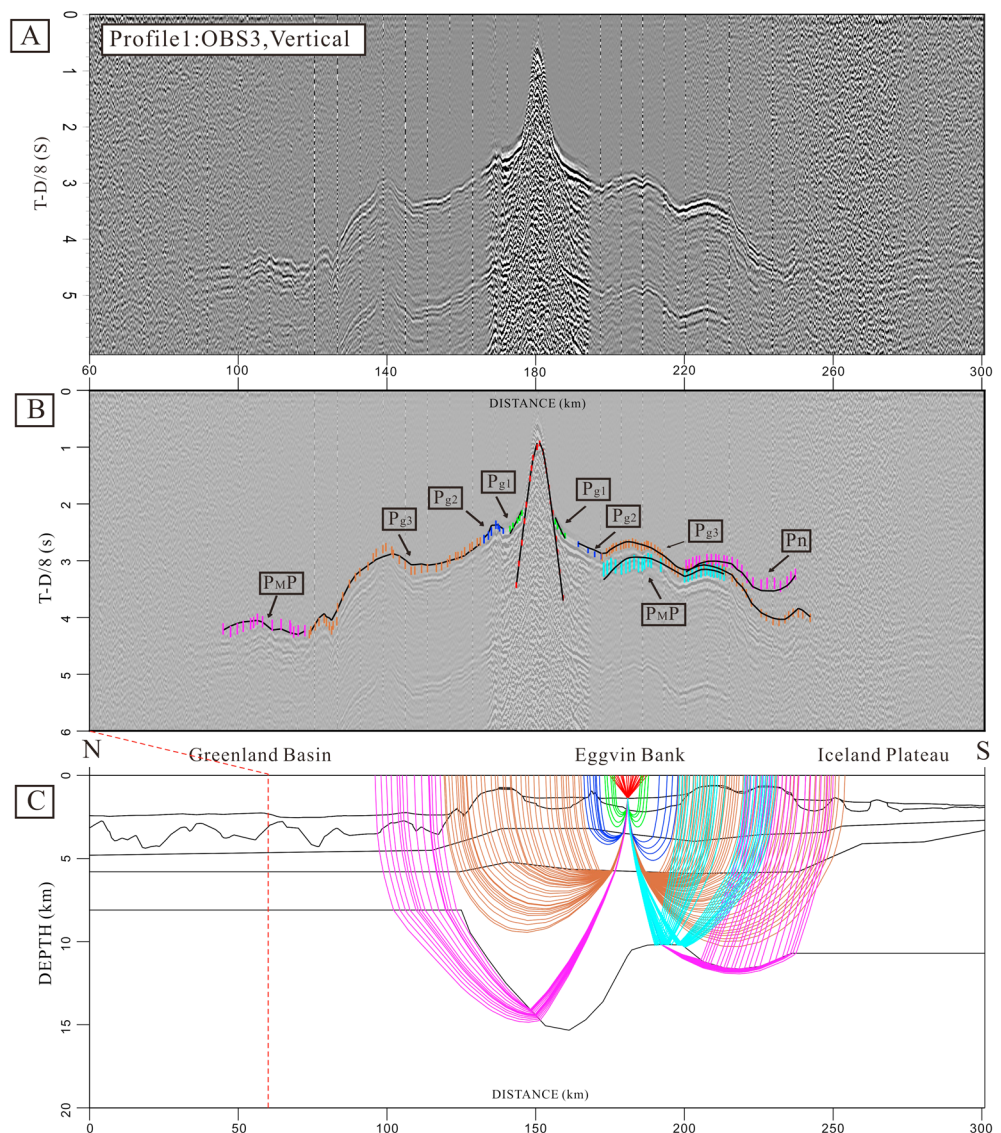
Figure 5. Data, interpretation, and ray tracing of OBS2. (a) Vertical component data of OBS2 reduced by 8 km/s (5–12 Hz band-pass filtered and offset-dependent scaling). (b) Comparison between calculated (black solid line) and interpreted traveltime (colored vertical bars) for OBS2 with data in the background. (c) Ray tracing of the velocity model.

south (190 km–235 km) is constrained by P_n and a few Moho reflections (P_mP) of OBSs 1–3 to a maximum of around 10 km. The velocity of the lower crust (layer 3) is controlled in this part of the model by P_{g3} phases (6.7 km/s to 7.35 km/s). The upper mantle velocity is at 7.7 km/s unusually low under the northern seamount. There is some freedom in the model to reduce Moho depth and lower crustal velocity here but that would require even lower mantle velocity. Ray tracing through inverse modeling by adjusting a set of selected lower crustal velocities, Moho depth, and upper mantle velocities in this region show the best fit for a velocity of 7.7 and 7.35 km/s in the upper mantle and lower crust, respectively. The southern 100 km of the model covers thinner ocean crust (8.5 km), where the velocity in the lower crust (layer 3) ranges from 6.7 to 7.15 km/s and the upper mantle velocity is estimated to 7.9–7.95 km/s. This result is consistent with the study of the nearby Iceland Plateau [*Kodaira et al.*, 1997, 1998a].

Based on the average velocity of each layer, Figure 9 represents the crustal velocity anomalies between 135 km and 301 km. In the upper crustal layer, low-velocity anomalies are found beneath the seamounts at the Eggvin Bank. The velocity anomalies in the two main peaks at 135–150 km and 200–220 km have amplitudes of −0.1 km/s and −0.3 km/s respectively, while the amplitude increase to −0.4 km/s under the

Figure 6. Data, interpretation and ray tracing of OBS3. (a) Vertical component data of OBS3 reduced by 8 km/s (5–12 Hz band-pass filtered and offset-dependent scaling). (b) Comparison between calculated (black solid line) and interpreted traveltime (colored vertical bars) for OBS3 with data in the background. (c) Ray tracing of the velocity model.

smaller peak between 160 km and 175 km. The near-surface velocities under the seamounts at 200–220 km and 160–175 km are mainly constrained by P_{g1} and P_{g2} from OBS2 (Figure 5) and P_{g2} from OBS3 (Figure 6), respectively. The variations in near-surface velocities may be associated with the formation ages of the seamounts. The low-velocity anomalies may indicate relatively young extrusives with high porosity and low degree of compaction [*Jacobson*, 1992; *Hooft et al.*, 2006], while the porosity could be reduced by cementation processes for older extrusives. Strong discontinuous reflections observed between 140 km and 190 km in the sediments may represent intrusions or lava flows, indicating that magmatic activity occurred after some sedimentation had taken place (Figure 3). Upper crustal velocities start to increase at the southernmost peak of the Eggvin Bank and become up to 0.4 km/s higher than average past 255 km. The middle crustal high velocity ($\leq$0.2 km/s) found in the central Eggvin Bank (175–230 km) may be due to the presence of high density basaltic intrusives [*Menke et al.*, 1998]. In addition, the upper and middle/lower crust (layer 2/layer 3) thickness ratio varies from 1:1 to 1:3 from the Eggvin Bank to the Iceland Plateau, indicating more extrusives at the Eggvin Bank. The lower crust velocity anomalies in the Eggvin bank have large variations between the two crustal roots. The northern root between 135 and 190 km has an up to 0.15 km/s increase, while the
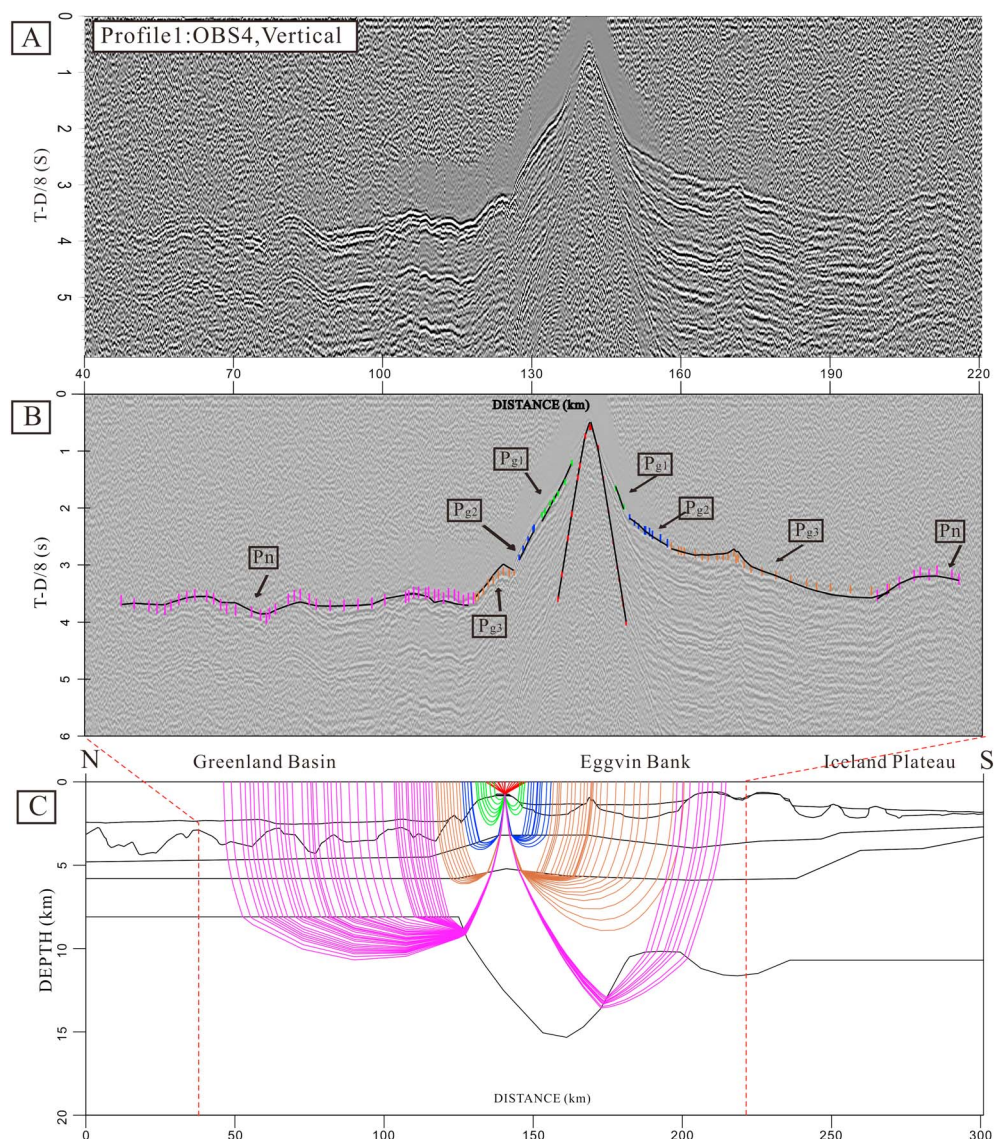
Figure 7. Data, interpretation, and ray tracing of OBS4. (a) Vertical component data of OBS4 reduced by 8 km/s (5–12 Hz band-pass filtered and automatic gain control (2 s window) scaling). (b) Comparison between calculated (black solid line) and interpreted traveltime (colored vertical bars) for OBS4 with data in the background. (c) Ray tracing of the velocity model.

southern root (190 km–235 km) structure is −0.1 km/s below average. This variation may indicate different melting degrees or source in these two areas.

### 4.2. *P* Wave Model Resolution and Uncertainties

The ray coverage density (2.5 by 0.25 km distance-depth grid) is shown in Figure 10a. Areas near OBSs and the upper parts of the lower crust have the highest ray coverage density. In order to estimate the model sensitivity to nodes, we determined the resolution values of the *P* wave velocity and depth nodes of both upper and lower boundaries by using the inversion function of Rayinvr [*Zelt and Smith*, 1992]. We show gridded velocity resolution values in Figure 10b. Depth node resolution is also indicated by the size of the circle enclosing it, larger meaning better constraints. The upper crustal (layers 2A, 2B) velocities, which are constrained by short offset refracted arrivals (P_{g1}, P_{g2}), are not highly resolved at distance from the OBSs. The best velocity constraints are found at upper parts of lower crust (layer 3) from 205 km to 250 km. The upper and middle crust (layers 2A, 2B) depth nodes in most parts of the Eggvin Bank (135–235 km) are well constrained (average above 0.5), while the Moho depth nodes are less well constrained. The best Moho depth constraints are found at the WJMFZ and at the southern Eggvin Bank.
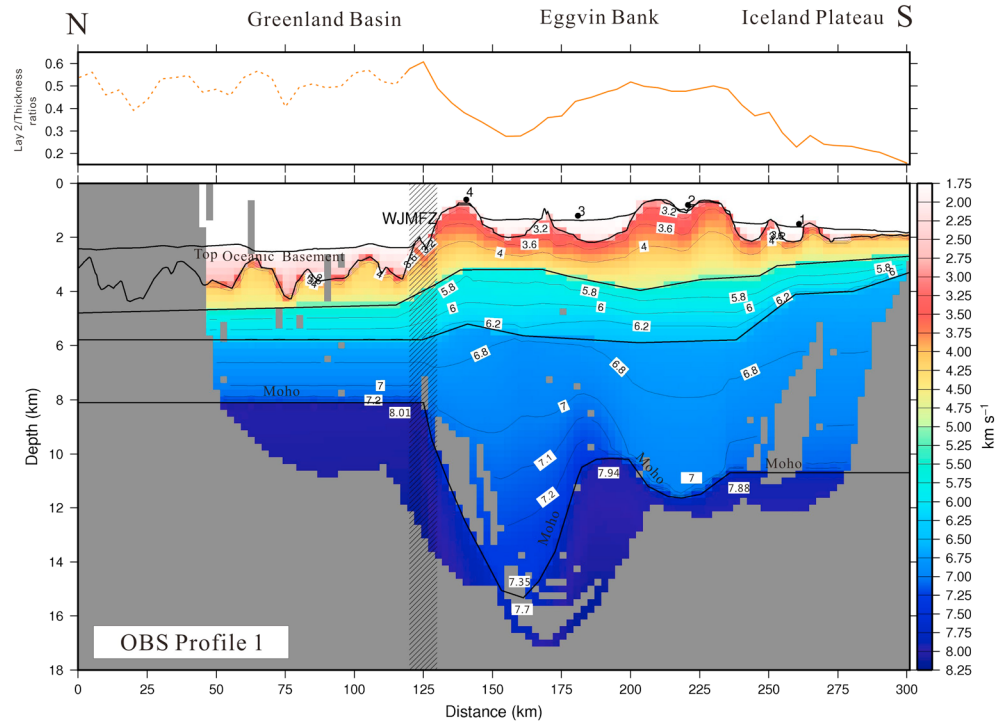
Figure 8. Gridded crustal velocity model of Profile-1. The area not covered by rays is masked. The OBS locations are illustrated on the seafloor with numbers. The West Jan Mayen Fracture Zone (WJMFZ) is presented by hachures. Velocity contour interval is 0.4 km/s in the upper crust, 0.2 km/s in the middle crust, and 0.1 km/s in the lower crust. The velocities of the upper mantle are also shown. V_P velocities are given by small numbers. The layer 2 thickness/total crustal thickness ratio along profile is shown above.

To quantify the uncertainties of the lower crustal velocity and Moho depth, we use an automated search through a range of selected lower crustal velocity nodes and Moho depth nodes (using P_{g3}, P_MP, and P_n phases). Changes in Moho depth can be accommodated with changes in V_p in the lower crust and still produce a reasonable fit. In each step, depth nodes are changed by 0.1 km, while velocity nodes will go through all iterations over a selected interval at 0.01 km/s steps. The fit statistics are documented after running through
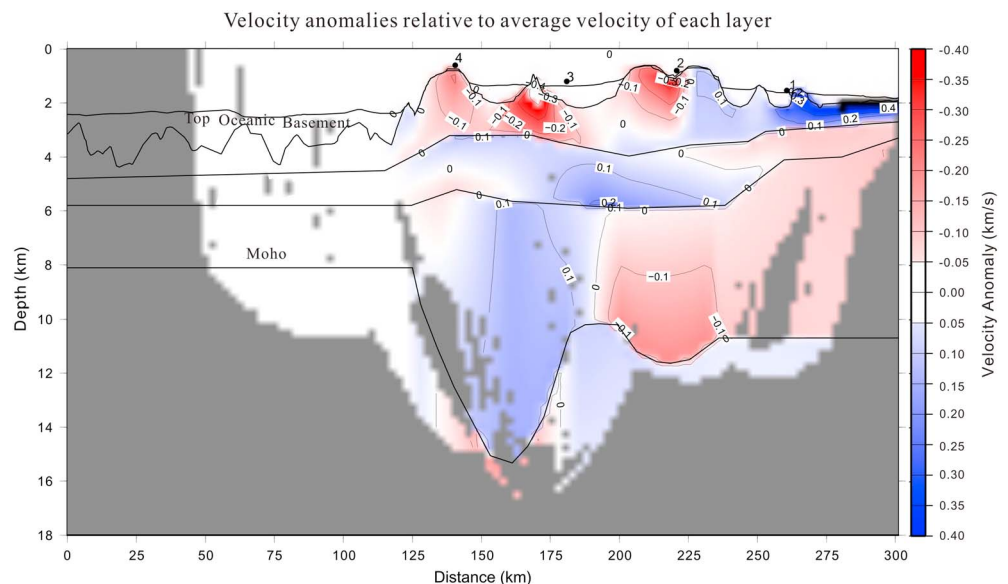

Figure 9. Velocity anomalies relative to mean velocity of each layer between 120 km and 301 km.
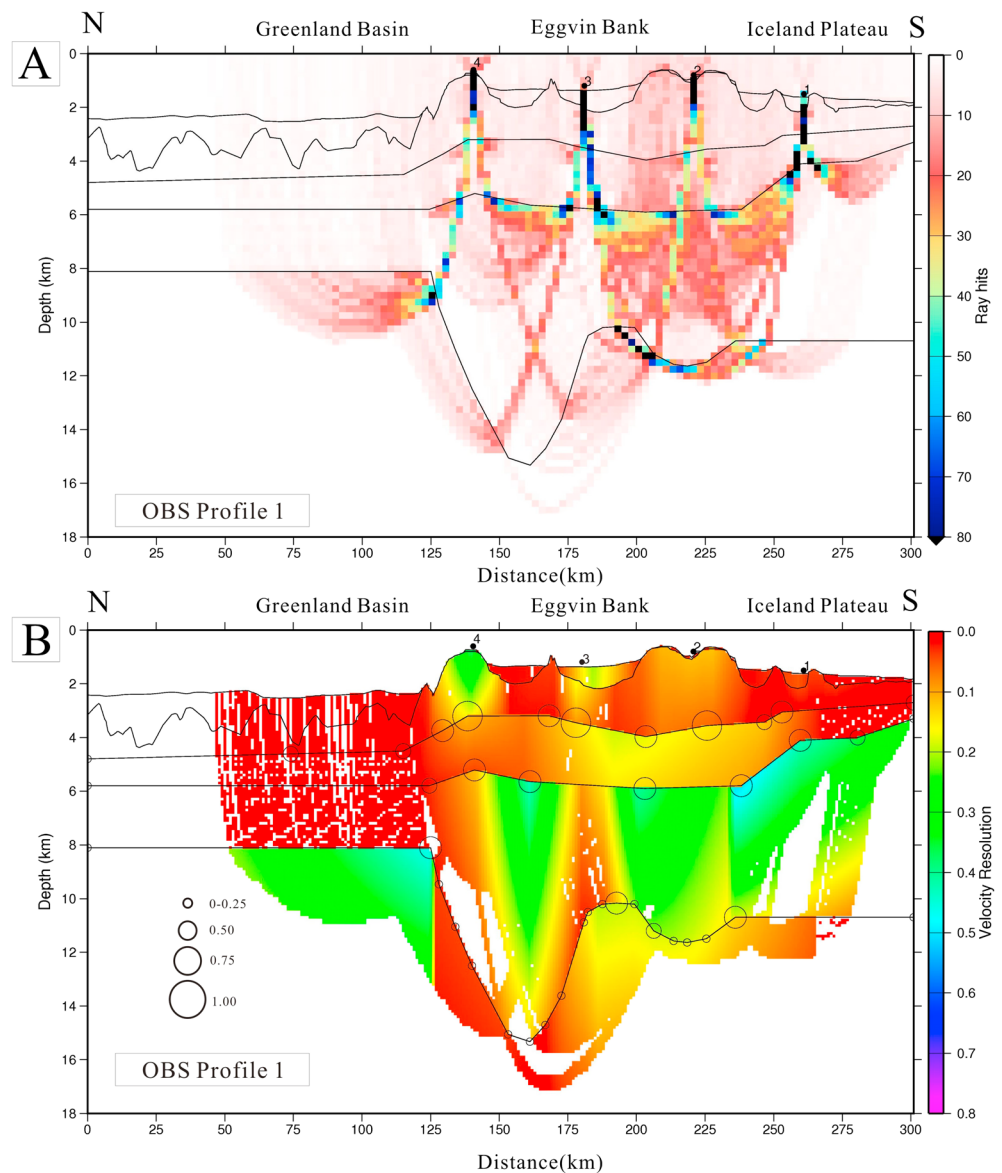
Figure 10. Ray coverage, velocity and depth node resolution. (a) Gridded ray coverage within a 2.5 by 0.25 km distance-depth grid. (b) Gridded *P* wave resolution parameters obtained from ray tracing inversion modeling. *P* wave velocity node resolution is shown by color, while depth node resolution is illustrated by the circle size.

the chosen intervals between 135 and 190 km and between 190 and 235 km, 8183 different models in total. This gives a good indication of the maximum range of velocity and Moho depth within a reasonable fit for the crustal roots at the northern and southern Eggvin Bank separately [e.g., *Breivik et al.*, 2012, 2014]. The contoured χ^2 and RMS Δt are summarized in Figure 11. The loss of rays is indicated by the background shading. It starts at 1 percent loss and reaches black at 10 percent loss. Based on $\chi^2 \leq 1$ and few rays lost, we estimate model uncertainties at the northern Eggvin Bank (135–190 km) to be −0.8/2.5 km for Moho depth and −0.4/0.35 km/s for the lower crustal velocity. For the southern Eggvin Bank (190–235 km), the uncertainties of the Moho depth and lower crustal velocity are estimated to be −1.1/1.5 km and ±0.3 km/s. Other geophysical data (e.g. gravity data) and isostasy analysis can sometimes supply further constraints. However, the uncertainty in lower crustal/upper mantle velocities and Moho depth will translate into a similar uncertainty in lower crustal/upper mantle densities and Moho depth. Additional uncertainties come from the expected changes of the lithospheric temperature/density structure next to the transform and the unconstrained depth extent of the upper mantle velocity/density anomaly. Therefore, a gravity/isostasy model is not expected to reduce the seismic model uncertainty.
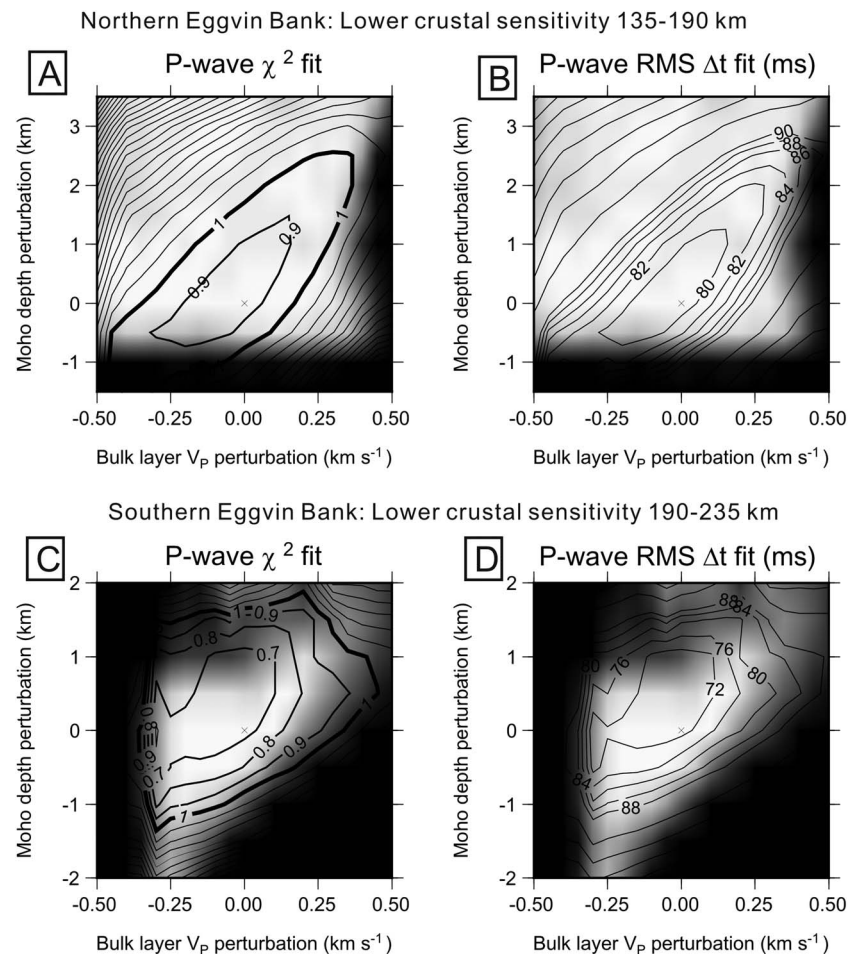
Figure 11. *P* wave model sensitivity to lower crustal velocity variations against Moho depth based on P_{g3}, $P_M P$, and P_n phases. Model sensitivity for the (a and b) northern Eggvin Bank and (c and d) southern Eggvin Bank. Increasing dark gray shading represents increasing loss of rays; black is at 10 percents loss.

4.3. *S* Wave Modeling

The *S* wave data is extracted from the horizontal components of the OBS instruments. The orientation of the horizontal components is arbitrary on the seafloor but can be estimated from a 3-D polarization analysis [*Maercklin*, 2007]. The two horizontal components are separately rotated into radial and transverse directions. The *S* wave energy will then be in the radial in-line direction mostly. Reorienting the instrument may therefore improve the S/N ratio.

In this study, the horizontal components of OBS1, OBS3, and OBS4 have been reoriented 305°, 202°, and 179° respectively, while OBS2 contained only one horizontal component with useful reading. Two types of *S* wave phases (PPS and PSS waves) have been identified from the horizontal components. PPS waves propagate initially as *P* waves and are converted into *S* waves at an interface within the crust on the way up, whereas PSS waves are converted on the way down, often at the seafloor or top basement. PSS phases give a direct estimate of the V_s in the crust, while PPS waves can give an indirect estimate in layers based on the delay time.

A velocity reduction of 8 km/s was applied to identify PPS waves, while the identification of PSS waves is based on a velocity reduction of 4.6 km/s. The data from the latter are shown in Figure 12a. The *S* wave modeling is based on the *P* wave velocity model geometry. By assigning a Poisson's ratio to each layer and determining the location of *P-S* conversion for each arrival, the *S* wave velocity can be estimated [*Zelt and Ellis*, 1988; *Zelt and Smith*, 1992]. The PSS arrival picks and modeled fit of all OBSs are shown in Figures 12b and 12c. The PSS modeling has shown that all of the *P-S* conversions occurred at top basement. The model is constrained by *S* waves in the lower crust (S_{g3}) and in the upper mantle (S_n). The interpretation uncertainties of the *S* wave arrivals from the lower crust and upper mantle are estimated to ±100 ms and ±200 ms, respectively. PSS wave
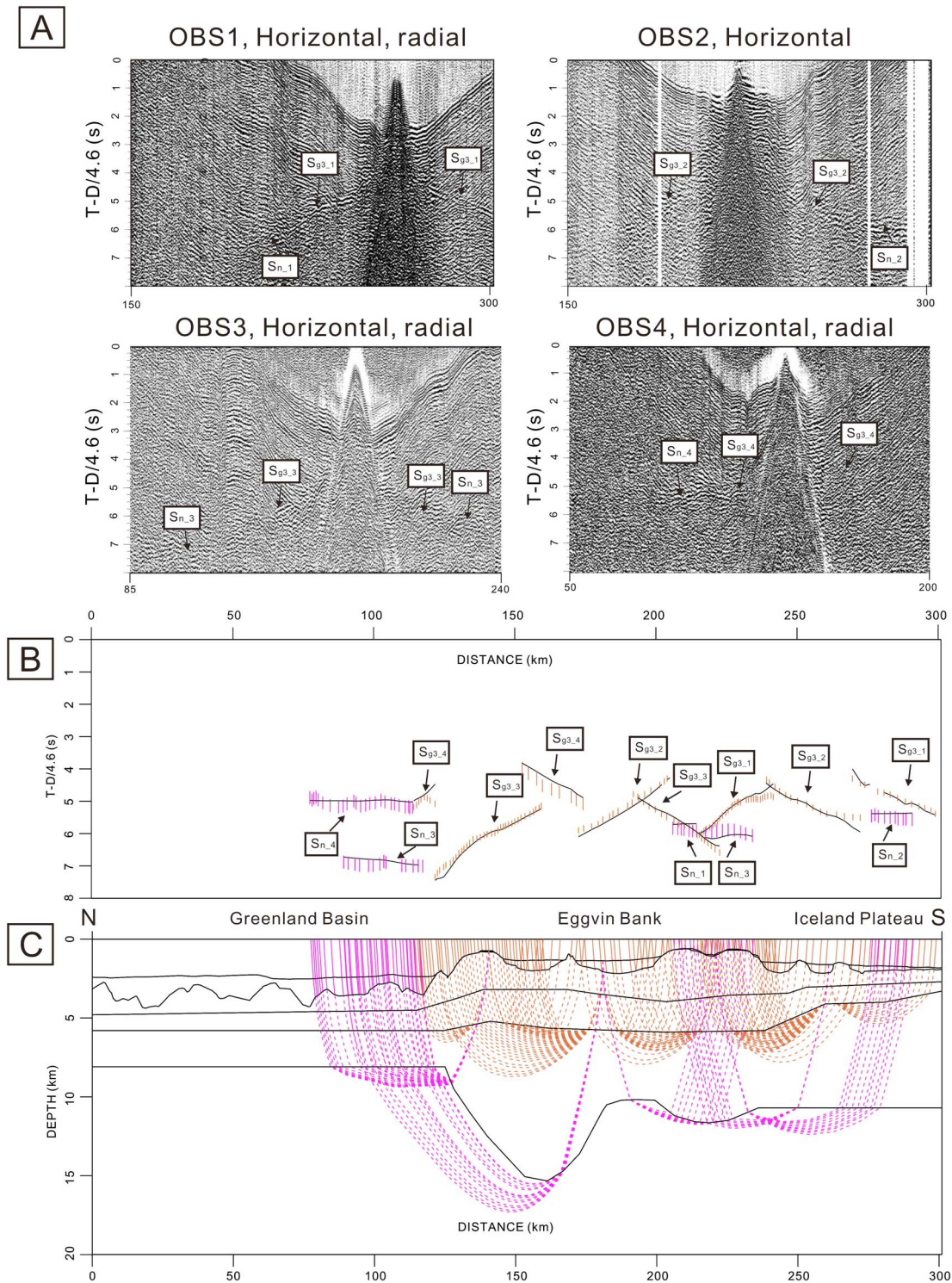
Figure 12. Horizontal, radial data (nonreoriented OBS2), PSS interpretation, and ray tracing of OBS1 to OBS4. (a) Horizontal component data for OBS1–OBS4 reduced by 4.6 km/s and phase identifications are shown on the recording section. (b) Comparison between calculated (black solid line) and interpreted traveltime (colored vertical bars). S_{g3_a}: S wave in lower crust in OBSa; S_{n_a}: S wave in the upper mantle in OBSa (a is 1, 2, 3, 4). (c) Ray tracing of the velocity model. The solid lines show P wave paths, while the dashed lines represent the S wave travel paths.

**Table 2.** Seismic Model Fit Statistics for Individual Major Phases (PSS Wave) and Summary For All Phases

Phase	No. rays	RMS Δt (ms)	χ^2
S_{g3}	144	100	1.006
S_n	74	143	0.515
All phases	218	117	0.826

fit statistics are summarized in Table 2. The P and S wave velocity modeling results are used to generate a V_p/V_s ratio model (Figure 13). The upper parts of the lower crust and the southern crustal root have the highest ray coverage density. The sediments in Eggvin Bank and Iceland Plateau have high V_p/V_s ratios (4.2 to 7.14) (constrained by PPS waves), which is interpreted as high porosity, uncompacted sediments [e.g., *Mjelde et al.*, 2003]. Due to the presence of quartz, the V_p/V_s ratio of felsic crystalline rocks (1.71) is smaller than mafic crystalline rocks (1.84) [e.g., *Holbrook et al.*, 1992]. The relatively high V_p/V_s ratios (1.82–1.88) for the crust indicate a mafic composition, and there is no obvious signature of continental crust extending from JMMC [*Campsie et al.*, 1990]. This is consistent with the typical oceanic crust observed in the P wave velocity model and agrees with the proposed COB of both *Breivik et al.* [2012] and *Peron-Pinvidic et al.* [2012a, 2012b] (Figure 2). The upper and middle crust have higher V_p/V_s ratios (1.87–1.88) than the lower crust (1.82–1.85). This difference is most likely due to a decreased fracture density with depth [*Mjelde et al.*, 2002]. In the Eggvin Bank, the upper and middle crust have similar V_p/V_s ratios, while lower crust shows variations between different regions. The upper mantle V_p/V_s ratio increases under the northern crustal root, but the ray coverage is low there.

5. Discussion

5.1. The Cause of Excess Magmatism

Wide-angle refraction studies along other portions of the Kolbeinsey Ridge indicate a relatively smooth increase in crustal thickness toward Iceland (Figure 14). Crustal thickness along the Southern Kolbeinsey Ridge (SKR) increase up to 13 km toward Iceland [*Hooft et al.*, 2006]. The crustal thickness adjacent to the Middle Kolbeinsey Ridge (MKR) axis appears to be slightly more variable with an average of about 9–9.5 km [*Kodaira et al.*, 1997]. Furthermore, the crust formed at the MKR shows no significant lateral variations in the igneous crustal thickness since 22 Ma [*Kodaira et al.*, 1998b]. However, the crustal thickness of the Eggvin Bank shows large variations, from 8 km to 13 km. This thick crust is also in agreement with a recent 3-D crustal model based on seismically constrained gravity inversion, where the crustal thickness over the Eggvin Bank is estimated to 10–15 km [*Haase et al.*, 2016]. In contrast to the Eggvin Bank, the southern transects show little lower crustal velocity variation. The northern Eggvin Bank has 0.2 km/s higher lower crustal velocity and 3 km thicker crust compared with southern Eggvin Bank (190–220 km) (Figure 9). While there is some uncertainty
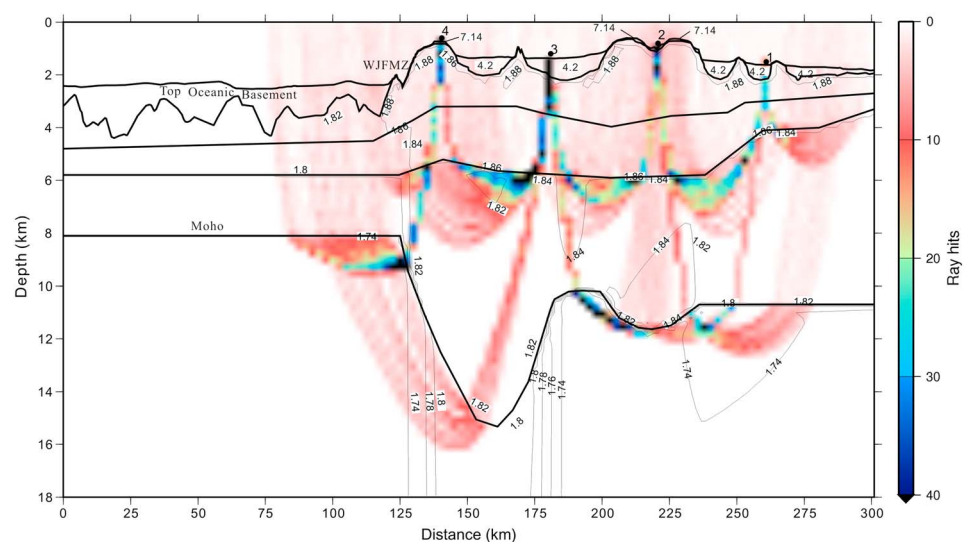
Figure 13. Contoured V_p/V_s ratios based on V_p and V_s velocity modeling. The background picture shows the V_s gridded ray coverage (2.5 by 0.25 km distance-depth grid).
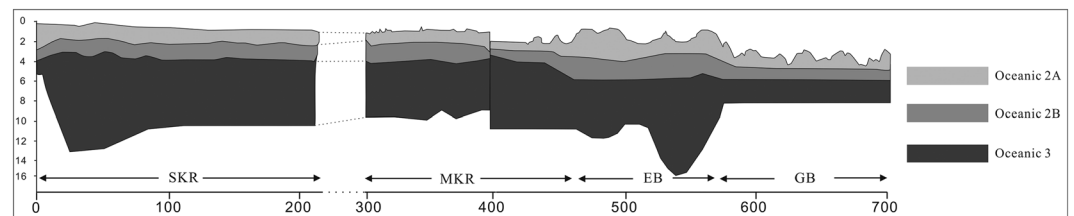
Figure 14. Combined transect from SKR to Eggvin Bank. The location is shown in Figure 1. The crustal profile of SKR and MKR is derived from *Hooft et al.* [2006] and *Kodaira et al.* [1997], respectively. The Eggvin Bank is from this study. The Eggvin Bank profile is on older crust and therefore deeper. The layers from top to bottom are oceanic 2A, oceanic 2B, and oceanic 3. SKR: South Kolbeinsey Ridge, MKR: Middle Kolbeinsey Ridge, EB: Eggvin Bank, GB: Greenland Basin.

to how pronounced this difference is, it could indicate changes in magmatic processes and how these affect total magma production and composition along profile. Both mantle composition and mantle melting degree will be important in that respect. A high melt degree caused by high mantle temperature results in melts with high MgO content relative the FeO content, yielding thick, high-velocity igneous crust [e.g., *White*, 1989; *Kelemen and Holbrook*, 1995; *Korenaga et al.*, 2002; *Sallarès et al.*, 2005]. If the crust is created on axis over a hot mantle plume, there will be a positive correlation between the crustal thickness and seismic velocity [*Holbrook et al.*, 2001]. High mantle upwelling rates (active upwelling relative to passive upwelling driven by seafloor spreading) lead to increased mantle volumes circulating through the melting zone. For a constant mantle temperature this will yield thicker oceanic crust with little change in seismic velocity as thickness changes [*Holbrook et al.*, 2001; *White et al.*, 2008]. On the other hand, if crustal thickness variations were only caused by the presence of a fertile mantle component in the melting zone, this would result in a negative correlation between crustal thickness and seismic velocity [e.g., *Korenaga et al.*, 2002; *Sallarès et al.*, 2005]. These three end-member models are valid for a single melt event, such as at a seafloor spreading axis. If a thick crust is created by multiple, low-degree melting events, FeO would most likely be high, and the velocity would be lower and resemble the result of active upwelling or of an extra fertile mantle.

5.2. H-V_p Analysis

The connection between the seismic properties that can be measured in igneous crust and the underlying mantle melting processes can be estimated based on the correlation between seismic velocity and crustal thickness (H-V_p analysis) [e.g., *Holbrook et al.*, 2001]. The average velocity of upper and middle crustal layers (layer 2) is strongly influenced by fissures and cracks [*Wilkens et al.*, 1991; *Jacobson*, 1992]. The lower crust (layer 3) is dominated by unaltered, low porosity gabbroic rocks, where velocity is mainly controlled by compositional variations.

We have used the pressure corrections from *Holbrook et al.* [2001] to calculate the average lower crustal velocities (Figure 15). For the temperature correction, we assume 10°C at the seafloor with 520°C fixed at 20 km depth and a linear gradient [*Tan et al.*, 2016]. Following *Holbrook et al.* [2001], we assigned all crustal velocities below 6.85 km/s to the value of 6.85 km/s to eliminate the effect of porosity.

5.3. H-V_p Results

The relationship between average lower crustal velocities and total crustal thickness is shown in Figure 15. Based on the best fit model, the northern Eggvin Bank has a positive H-V_p correlation, while the southern Eggvin Bank shows a poor H-V_p correlation. In the northern Eggvin Bank, the crustal thickness increase from 8 km to 13 km associated with a V_p increase of 0.1 km/s to just above 7.0 km/s. The southern Eggvin Bank, however, has a low velocity (around 6.85 km/s for crustal thickness exceeding 10 km), where the V_p remains almost unchanged over crustal thickness variations of 8 km to 11 km.

Based on the sensitivity analysis (Figure 11), the minimum (the shallowest Moho and lowest lower crustal velocity) and maximum velocity models (the deepest Moho and highest lower crustal velocity) show large variations of the H-V_p correlations (Figure 15b). The northern Eggvin Bank maximum velocity model shows a positive H-V_p correlation with larger crustal thickness and high lower crustal V_p. However, the minimum velocity model has a more horizontal H-V_p pattern, similar to southern Eggvin Bank. These different H-V_p patterns would require different mantle melting processes. We prefer the positive H-V_p correlation in the northern Eggvin Bank, but a horizontal H-V_p pattern cannot be completely ruled out. Both the maximum and minimum velocity models of the southern Eggvin Bank have a poor H-V_p correlation with low average V_p.
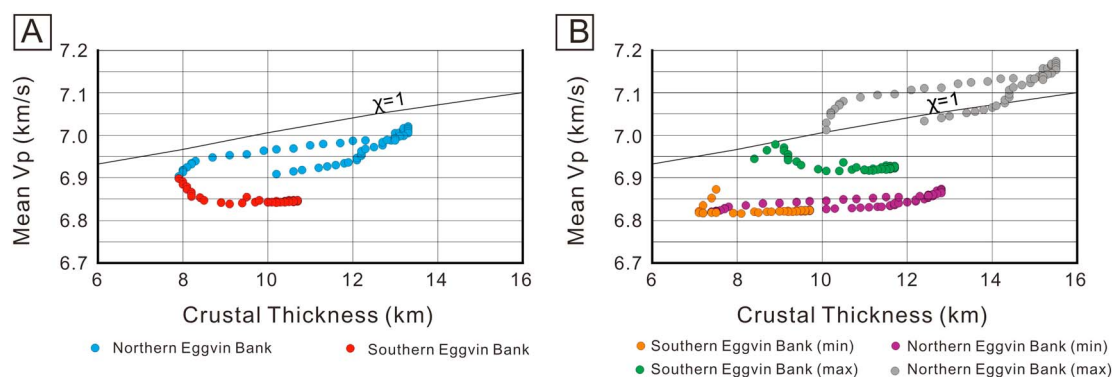
Figure 15. Crustal thickness versus mean V_p for the Eggvin Bank. Sampling interval is 1 km horizontally. (a) The northern Eggvin Bank comprises the region from 135 km to 190 km, while the southern Eggvin Bank is the region from 190 km to 220 km. $\chi=1$ shows passive decompression melting of normal mantle with increasing temperature [*McKenzie and Bickle*, 1988]. The pressure corrections used by *Holbrook et al.* [2001], while the temperature correction assume a linear gradient from 10°C at the seafloor to 520°C at 20 km depth [*Tan et al.*, 2016]. (b) Minimum and maximum velocity models indicated by the sensitivity analysis (Figure 11).

If real, the positive H-V_p correlation for the northern Eggvin Bank (Figure 15a) may have two alternative explanations. If the entire crustal section was created at the spreading center, it would represent a single melting event governed by elevated mantle temperature. However, another scenario involving additional off-axis melting could still result in a positive H-V_p correlation. If one of the major melting episodes are driven by excess temperature, the next episode would not necessarily overprint the positive H-V_p correlation. If that happened, most likely the primary oceanic crust formed at the spreading center (on-axis event) should have high Mg/Fe ratios (high degrees of melting) and the secondary addition to the igneous crust may results from relatively lower degrees of melting, which is expected since the thicker lithosphere will result in a shorter melt extraction column and the residual asthenosphere has become more refractory.

A poor H-V_p correlation of the southern Eggvin Bank indicates that the lower crustal composition changes little with crustal thickness variations [e.g., *White*, 1989]. If all crust was formed on axis, that would require active upwelling with low-degree melting and/or enriched components to explain excess crustal thickness. However, multiple melting events with crustal off-axis additions generated by relatively low degree of partial melting could also result in basalts with low Mg/Fe ratio and a poor H-V_p correlation [e.g., *Yaxley*, 2000; *Korenaga et al.*, 2002]. To what degree this also applies to the north is uncertain, but it could be noted that both curves are low in the diagram, consistent with multiple melting events.

The layer 2 thickness of SKR and MKR is uniformly 3.5 km thick (Figure 14). Along the Eggvin Bank, layer 2 is slightly thicker (4.2 ± 0.5 km), whereas layer 3 is considerably more variable and thicker (4.5 – 9.5 km). Clearly, there has been significantly more of extrusive magmatism at the Eggvin Bank creating the seamounts. Normal oceanic crust, which is formed at a seafloor spreading axis through a single melting event, has generally a uniform proportion of layer 2 to total crustal thickness of around 25%, so that most of the crustal thickening is accommodated by layer 3 [*Korenaga et al.*, 2000; *Sallarès et al.*, 2003; *Hampel et al.*, 2004; *Sallarès et al.*, 2005]. However, the proportion of layer 2 for off-axis crust, created by multiple melting events, is mostly around 50% [*Watts and Ten Brink*, 1989; *Caress et al.*, 1995; *Charvis et al.*, 1999; *Ye et al.*, 1999; *Canales et al.*, 2000]. Along the Eggvin Bank profile, the average ratio of layer 2 thickness versus total crustal thickness is 0.36 in the northern region, while it is 0.46 in southern region (Figure 8). Minimum and maximum models give ratios of 0.29 to 0.39 in the north. In the south it varies from 0.44 to 0.52. The high ratio both in the north and the south indicates that the formation of the seamounts is probably not at the spreading center. The northern seamount has a flat top (730 m deep), which indicates that it has been eroded above or near sea level, while in the south the profile crosses the summit of the shallowest one, which has a rounded top of 460 m depth, even if the crust is 3 – 4 Ma older. The southernmost seamount has a depth of 550 m on the profile, but it is located slightly to the side of the summit. These observations suggest that the southern seamounts are younger, since they are shallower but without obvious signs that they were subaerially exposed. This indicates that the southern but possibly also the northern Eggvin Bank is created by multiple melting events on and off axis and that the southern Eggvin Bank seamounts have a younger formation age than the northern seamount.

5.4. Upper Mantle Velocities

The anomalously low V_p (7.7 km/s) as well as relatively high V_p/V_s ratios (1.8) in the upper mantle observed in the northern region (140 km–170 km) (Figures 8 and 13) could represent partial serpentinization of mantle material [e.g., *Bown and White*, 1995; *Mjelde et al.*, 2002; *Fujie et al.*, 2013]. If the mantle serpentinization is due to the influence of WJMFZ, it is most likely to occur along the fracture zone. However, the relatively high V_p (8.01 km/s) and lower V_p/V_s ratios (1.73) in the mantle under the WJMFZ indicate that the anomalous V_p and V_p/V_s ratio in the upper mantle south of it are due to other factors. Lower velocities in the upper mantle could also be interpreted as melt retention in the upper mantle [e.g., *Cannat*, 1996]. Based on mineralogical studies, *Haase et al.* [2003] pointed out that the WJMFZ could cool the ascending magmas by up to 100°C compared to southern NKR. This could have increased the effect of conductive cooling and made melt extraction less effective, with more melt solidified in the upper mantle [e.g., *Lizarralde et al.*, 2004]. The elevated V_p/V_s ratio in the uppermost mantle (Figure 13) supports melt retention, since gabbro has a higher ratio than peridotite [*Christensen*, 1996].

5.5. Geochemistry of the Eggvin Bank

None of the seamounts along Profile-1 have been sampled, although several studies have sampled younger seamounts nearby as well as the seafloor spreading axis (Figure 2). The dredged samples from NKR, near-axis, and off-axis seamounts at the Eggvin Bank are enriched in incompatible elements [*Campsie et al.*, 1990; *Haase et al.*, 2003; *Mertz et al.*, 2004; *Elkins et al.*, 2011, 2016]. This indicates elevated proportions of enriched source components under the NKR and surrounding Eggvin Bank at the present and probably also in the past. The NKR basalts are isotopically similar to basalts from sources with recycled oceanic crust, erupted in the southern Flank Zone and on the Reykjanes Peninsula in Iceland [e.g., *Mertz et al.*, 2004; *Debaille et al.*, 2009; *Trønnes et al.*, 2013], whereas the off-axis Eggvin Bank basalts are compositionally intermediate between basalts from the Jan Mayen area and the NKR. An enriched mantle source appears to be the main reason for the anomalous magmatism at the Eggvin Bank and may also determine the location of the spreading ridge offset from the MKR. Source variations could have produced differences in the magmatism between northern and southern parts of the Eggvin Bank in the past. The southern part should be dominated by an enriched mantle source, since the crust was likely formed by multiple melting events with lower mantle melting degrees. However, the northern part shows signs of mantle melting driven by elevated temperature, where the enriched mantle source may have played a lesser role.

The northeast Atlantic region has been significantly influenced by the Iceland plume to varying degrees since the time of continental breakup [e.g., *Hooft et al.*, 2006; *Howell et al.*, 2014]. Isotopic constrains, thermal anomalies, and V-shaped ridges suggest that the Iceland plume affects the entire length of the Kolbeinsey Ridge [*Poreda et al.*, 1986; *Jones et al.*, 2002; *Pilidou et al.*, 2005]. As demonstrated by *Mertz et al.* [2004], dispersion of enriched material from a putative Jan Mayen plume cannot explain the radiogenic Nd-Pb isotope compositions of basalts from the Eggvin Bank and the NKR. These basalt compositions, however, are consistent with sources emplaced by deep-level northward flow of Iceland plume material, ascending into the melting zone south of the WJMFZ.

6. Summary and Conclusions

The crustal structure of the Eggvin Bank has been investigated from refraction/reflection data along one seismic profile. Results from *P* wave traveltime modeling show oceanic crustal velocities, with a low-velocity upper crust (2.8 km/s to 4.8 km/s), a middle crust (5.5 km/s to 6.5 km/s), and a low-gradient, high-velocity lower crust (6.7 km/s to 7.35 km/s). These typical oceanic crustal velocities and relatively high crustal V_p/V_s ratios (1.82–1.88) indicate a mafic composition and are inconsistent with continental crust extending from the JMMC to the Eggvin Bank. However, the anomalously thick crust and the morphology of the Eggvin Bank differ from typical oceanic crust at the Kolbeinsey Ridge to the south. The crust has large variations in thickness, from 8 km to 13 km, where a 2–5 km increase is associated with two 20–30 km wide segments under the main seamounts.

Based on the increase of the layer 2 thickness and the high ratio of layer 2 thickness to total crustal thickness, we infer that secondary, intraplate magmatism probably played an important role in building the seamounts of the Eggvin Bank. The flat top of the seamount in the north indicates subaerial exposure despite being deeper and is therefore probably older than the shallower seamounts with rounded tops in the south.

We correlate lower crust seismic velocity (V_p) and crustal thickness (H) in order to estimate the formation mechanisms in the Eggvin Bank. Along Profile-1, the northern Eggvin Bank tends toward a positive H-V_p correlation, though there is some uncertainty to this result. This indicates that the northern Eggvin Bank could be created by higher degree of mantle melting driven by elevated temperature. The southern Eggvin Bank is characterized by an overall poor H-V_p correlation and low V_p in the lower crust, which is compatible with multiple melting events with low mantle melting degree. An enriched mantle source presently feeds the NKR magmatism, which may have influenced the development of the Eggvin Bank also at earlier times, being an important source for the off-axis magmatism. To what extent the Eggvin Bank has been influenced by the Iceland plume is uncertain, both an enriched mantle component and elevated mantle temperature may have played a role in its development at different times and locations.

References

Bown, J. W., and R. S. White (1995), Effect of finite extension rate of melt generation at rifted continental margins, *J. Geophys. Res.*, *100*, 18,011–18,029.

Breivik, A., R. Mjelde, J. I. Faleide, E. Flueh, and Y. Murai (2014), Magmatic development of the outer Vøring margin from seismic data, *J. Geophys. Res. Solid Earth*, *119*, 6733–6755, doi:10.1002/2014JB011040.

Breivik, A. J., R. Mjelde, P. Grogan, H. Shimamura, Y. Murai, and Y. Nishimura (2003), Crustal structure and transform margin development south of Svalbard based on ocean bottom seismometer data, *Tectonophysics*, *369*, 37–70.

Breivik, A. J., R. Mjelde, J. I. Faleide, and Y. Murai (2012), The eastern Jan Mayen microcontinent volcanic margin, *Geophys. J. Int.*, *188*, 798–818, doi:10.1111/j.1365-246X.2011.05307.x.

Campsie, J., M. H. Rasmussen, L. C. Kovacs, F. Dittmer, J. C. Bailey, N. O. Hansen, and L. Johnson (1990), Chronology and evolution of the northern Iceland Plateau, *Polar Res.*, *8*(2), 237–243.

Canales, J. P., J. J. Danobeitia, and A. B. Watts (2000), Wide-angle seismic constraints on the internal structure of Tenerife, Canary Islands, *J. Volcanol. Geotherm. Res.*, *103*, 65–81.

Cannat, M. (1996), How thick is the magmatic crust at slow spreading oceanic ridges?, *J. Geophys. Res.*, *101*, 2847–2857.

Caress, D. W., M. K. McNutt, R. S. Detrick, and J. Mutter (1995), Seismic imaging of hotspot-related crustal underplating beneath the Marquesas Islands, *Nature*, *373*, 600–603.

Charvis, P., A. Laesanpure, J. Gallart, A. Hirn, J. C. Lepine, B. de Voogd, Y. Hello, B. Pontoise, and T. A. Minshull (1999), Spatial distribution of hot spot material added to the lithosphere under La Reunion, from wide-angle seismic data, *J. Geophys. Res.*, *104*, 2875–2893.

Christensen, N. I. (1996), Poisson's ratio and crustal seismology, *J. Geophys. Res.*, *101*(B2), 3139–3156.

Christeson, G., G. Purdy, and G. Fryer (1994), Seismic constrains on shallow crustal emplacement processes at the fast spreading East Pacific Rise, *J. Geophys. Res.*, *99*, 17,957–17,974.

Debaille, V., R. G. Trønnes, A. D. Brandon, T. E. Waight, D. W. Graham, and C. A. Lee (2009), Primitive off-rift basalts from Iceland and Jan Mayen: Os-isotopic evidence for a mantle source containing enriched subcontinental lithosphere, *Geochim. Cosmochim. Acta.*, *73*, 3423–3449.

Detrick, R., J. Collins, R. Stephen, and S. Swift (1994), In situ evidence for the nature of the seismic layer 2/3 boundary in oceanic crust, *Nature*, *370*, 288–290.

Dilek, Y. (1998), Structure and tectonics of intermediate-spread oceanic crust drilled at DSDP/ODP holes 504B and 896A, Costa Rica Rift, in *Geolocial Evolution of Ocean Basin: Results From the Ocean Drilling Program, Geol. Soc. London, Spec. Publ.*, 131, 179–197.

Eldholm, O., and K. Grue (1994), North Atlantic volcanic margins: Dimensions and production rates, *J. Geophys. Res.*, *99*(B2), 2955–2968.

Elkins, L. J., et al. (2011), Understanding melt generation beneath the slow-spreading Kolbeinsey Ridge using ^{238}U, ^{230}Th, and ^{231}Pa excesses, *Geochim. Cosmochim. Acta*, *75*, 6300–6329.

Elkins, L. J., E. R. Rivers, K. W. W. Sims, J. Blichert-Toft, C. Devey, R. Chernow, R. Davis, and K. Meisenhelder (2013), Origins of anomalous ridge magmatism near Jan Mayen, *Mineral Mag.*, *77*(5), 1035.

Elkins, L. J., C. Hamelin, J. Blichert-Toft, S. R. Scott, K. W. W. Sims, I. A. Yeo, C. W. Devey, and R. B. Pedersen (2016), North Atlantic hotspot-ridge interaction near Jan Mayen Island, *Geochem. Persp. Lett.*, *2*, 55–67.

Engen, Ø., J. I. Faleide, and T. Karlberg Dyreng (2008), Opening of the Fram Strait gateway: A review of plate tectonic constraints, *Tectonophysics*, *450*, 51–69, doi:10.1016/j.tecto.2008.01.002.

Evans, J. R., and I. S. Sacks (1979), Deep structure of the Iceland Plateau, *J. Geophys. Res.*, *84*, 6859–6866.

Fujie, G., S. Kodaira, M. Yamashita, T. Sato, and N. Takahashi (2013), Systematic changes in the incoming plate structure at the Kuril trench, *Geophys. Res. Lett.*, *40*, 88–93, doi:10.1029/2012GL054340.

Funck, T., W. H. Geissler, G. S. Kimbell, S. Gradmann, M. K. Ö Erlendsson, and U. K. Petersen (2016), Moho and basement depth in the NE Atlantic Ocean based on seismic refraction data and receiver functions, *Geol. Soc. Spec. Publ.*, *477*, doi:10.1144/SP447.1.

Gaina, C., L. Gernigon, and P. Ball (2009), Palaeocene–Recent plate boundaries in the NE Atlantic and the formation of the Jan Mayen microcontinent, *J. Geol. Soc.*, *166*, 601–616, doi:10.1144/0016-76492008-112.

Gernigon, L., O. Olesen, J. Ebbing, S. Wienecke, C. Gaina, J. Mogaard, M. Sand, and R. Myklebust (2008), Geophysical insights and early spreading history in the vicinity of the Jan Mayen Fracture Zone, Norwegian-Greenland sea, *Tectonophysics*, *468*, 185–205.

Haase, C., J. Ebbing, and T. Funck (2016), A 3D crustal model of the NE Atlantic based on seismic and gravity data, *Geol. Soc. Spec. Publ.*, *447*, SP447-8, doi:10.1144/SP447.8.

Haase, K. M., C. W. Devey, and M. Wieneke (2003), Magmatic processes and mantle heterogeneity beneath the slow-spreading northern Kolbeinsey Ridge segment, North Atlantic, *Contrib. Mineral. Petrol.*, *144*, 428–448.

Hampel, A., N. Kukowski, J. Bialas, C. Huebscher, and R. Heinbockel (2004), Ridge subduction at an erosive margin-the collision zone of the Nazca Ridge in southern Peru, *J. Geophys. Res.*, *109*, B02101, doi:10.1029/2003JB002593.

Havskov, J., and K. Atakan (1991), Seismicity and volcanism of Jan Mayen Island, *Terra Nova*, *3*(5), 517–526.

Holbrook, W. S., W. D. Mooney, and N. I. Christensen (1992), The seismic structure of the deep continental crust, in *Continental Lower Crust*, edited by D. M. Fountain, R. Arculus, and R. W. Kay, pp. 1–43, Elsevier, Amsterdam.

Holbrook, W. S., et al. (2001), Mantle thermal structure and active upwelling during continental breakup in the North Atlantic, *Earth Planet. Sci. Lett.*, *190*, 251–266.

Hooft, E. E. E., R. S. Detrick, D. R. Toomey, J. A. Collins, and J. Lin (2000), Crustal thickness and structure along three contrasting spreading segments of the Mid-Atlantic Ridge, 33.5°–35° N, *J. Geophys. Res.*, *105*(B4), 8205–8226.

Hooft, E. E. E., B. Brandsdóttir, R. Mjelde, H. Shimamura, and Y. Murai (2006), Asymmetric plume ridge interaction around Iceland: The Kolbeinsey Ridge Iceland Seismic Experiment, *Geochem. Geophys. Geosyst.*, *7*, Q05015, doi:10.1029/2005GC001123.

Howell, S. M., G. Ito, A. J. Breivik, A. Rai, R. Mjelde, B. Hanan, K. Sayit, and P. Vogt (2014), The origin of the asymmetry in the Iceland hotspot along the Mid-Atlantic Ridge from continental breakup to present-day, *Earth Planet. Sci. Lett.*, *392*, 143–153.

Imsland, P. (1986), The volcanic eruption on Jan Mayen, January 1985: Interaction between a volcanic island and a fracture zone, *J. Volcanol. Geotherm. Res.*, *28*, 45–53.

Jacobson, R. S. (1992), Impact of crustal evolution on changes of the seismic properties of the uppermost oceanic crust, *Rev. Geophys.*, *30*(1), 23–42.

Jakobsson, M., et al. (2012), International Bathymetric Chart of the Arctic Ocean (IBCAO) version 3.0, *Geophys. Res. Lett.*, *39*, L12609, doi:10.1029/2012GL052219.

Jones, S. M., N. White, and J. Maclennan (2002), V-shaped ridges around Iceland: Implications for spatial and temporal patterns of mantle convection, *Geochem. Geophys. Geosyst.*, *3*(10), 1059, doi:10.1029/2002GC000361.

Kandilarov, A., R. Mjelde, R. B. Pedersen, B. Hellevang, C. Papenberg, C. J. Petersen, L. Planert, and E. Flueh (2012), The northern boundary of the Jan Mayen Microcontinent, North Atlantic determined from ocean bottom seismic, multichannel seismic, and gravity data, *Mar. Geophys. Res.*, *33*(1), 55–76.

Kandilarov, A., R. Mjelde, E. Flueh, and R. B. Pedersen (2015), V_p/V_s-ratios and anisotropy on the northern Jan Mayen Ridge, North Atlantic, determined from ocean bottom seismic data, *Polar Sci.*, *9*(3), 293–310.

Kelemen, P. B., and W. S. Holbrook (1995), Origin of thick, high-velocity, igneous crust along the U.S. East Coast Margin, *J. Geophys. Res.*, *100*(B7), 10,077–10,094.

Klingelhöfer, F., L. Géli, and R. S. White (2000), Geophysical and geochemical constraints on crustal accretion at the very-slow spreading Mohns Ridge, *Geophys. Res. Lett.*, *27*(10), 1547–1550.

Kodaira, S., R. Mjelde, H. Shimamura, K. Gunnarsson, and H. Shiobara (1997), Crustal structure of the Kolbeinsey Ridge, N. Atlantic, obtained by use of Ocean Bottom Seismographs, *J. Geophys. Res.*, *102*(B2), 3131–3151.

Kodaira, S., R. Mjelde, K. Gunnarsson, H. Shiobara, and H. Shimamura (1998a), Structure of the Jan Mayen microcontinent and implication for its evolution, *Geophys. J. Int.*, *132*, 383–400.

Kodaira, S., R. Mjelde, K. Gunnarsson, H. Shiobara, and H. Shimamura (1998b), Evolution of oceanic crust on the Kolbeinsey Ridge, north of Iceland, over the past 22 Myr, *Terra Nova*, *10*, 27–31.

Korenaga, J., W. S. Holbrook, G. M. Kent, P. B. Kelemen, R. S. Detrick, H. C. Larsen, J. R. Hopper, and T. Dahl-Jensen (2000), Crustal structure of the southeast Greenland margin from joint refraction and reflection seismic tomography, *J. Geophys. Res.*, *105*, 21,591–21,614.

Korenaga, J., P. B. Kelemen, and W. S. Holbrook (2002), Methods for resolving the origin of large igneous provinces from crustal seismology, *J. Geophys. Res.*, *107*(B9), 2178, doi:10.1029/2001JB001030.

Lizarralde, D., J. B. Gaherty, J. A. Collins, G. Hirth, and S. D. Kim (2004), Spreading-rate dependence of melt extraction at mid-ocean ridges from mantle seismic data, *Nature*, *432*, 744–747, doi:10.1038/nature03140.

Ljones, F., A. Kuwano, R. Mjelde, A. J. Breivik, H. Shimamura, Y. Murai, and Y. Nishimura (2004), Crustal transect from the North Atlantic Knipovich Ridge to the Svalbard margin west of Hornsund, *Tectonophyics*, *378*, 17–41.

Maercklin, N. (2007), *Supolar and supofilt: Su programs for polarization analysis and filtering of three-component data*.

Maus, S., T. Sazonova, K. Hemant, J. D. Fairhead, and D. Ravat (2007), National geophysical data center candidate for the world digital magnetic anomaly map, *Geochem. Geophys. Geosyst.*, *8*(6), Q06017, doi:10.1029/2007GC001643.

McKenzie, D., and M. J. Bickle (1988), The volume and composition of melt generated by extension of the lithosphere, *J. Petrol.*, *29*(3), 625–679.

Menke, W., M. West, B. Brandsdóttir, and B. Sparks (1998), Compressional and shear velocity structure of the lithosphere in northern Iceland, *Bull. Seismol. Soc. Am.*, *88*, 1561–1571.

Mertz, D. F., W. D. Sharp, and K. M. Haase (2004), Volcanism on the Eggvin Bank (Central Norwegian–Greenland Sea, latitude ∼71°N): Age, source, and relationship to the Iceland and putative Jan Mayen plumes, *J. Geodyn.*, *38*, 57–83, doi:10.1016/j.jog.2004.03.003.

Mjelde, R., R. Aurvåg, S. Kodaira, H. Shimamura, K. Gunnarsson, A. Nakanishi, and H. Shiobara (2002), V_p/V_s-ratios from the central Kolbeinsey Ridge to the Jan Mayen Basin, North Atlantic; implications for lithology, porosity and present-day stress field, *Mar. Geophys. Res.*, *23*(2), 123–145.

Mjelde, R., T. Raum, P. Digranes, H. Shimamura, H. Shiobara, and S. Kodaira (2003), V_p/V_s ratio along the Vøring margin, NE Atlantic, derived from OBS-data: Implications on lithology and stress-field, *Tectonophysics*, *369*, 175–197.

Mjelde, R., I. Eckhoff, S. Solbakken, S. Kodaira, H. Shimamura, K. Gunnarsson, A. Nakanishi, and H. Shiobara (2007), Gravity and S-wave modeling across the Jan Mayen Ridge, North Atlantic; Implications for crustal lithology and continental break-up processes, *Mar. Geophys. Res.*, *28*, 27–41, doi:10.1007/s11001-006-9012-3.

Morgan, W. (1983), Hotspot tracks and the early rifting of the Atlantic, *Tectonophysics*, *94*, 123–139.

Mosar, J., G. Lewis, and T. H. Torsvik (2002), North Atlantic sea-floor spreading rates: Implications of the Tertiary development of inversion structures of the Norwegian–Greenland Sea, *J. Geol. Soc.*, *159*, 503–515.

Noble, R. H., R. M. Macintyre, and P. E. Brown (1988), Age constraints on Atlantic evolution: Timing of magmatic activity along the E Greenland continental margin, *Geol. Soc. Spec. Publ.*, *39*, 201–214, doi:10.1144/GSL.SP.1988.039.01.19.

Peron-Pinvidic, G., L. Gernigon, C. Gaina, and P. Ball (2012a), Insights from the Jan Mayen system in the Norwegian–Greenland sea—I. Mapping of a microcontinent, *Geophys. J. Int.*, *191*, 385–412.

Peron-Pinvidic, G., L. Gernigon, C. Gaina, and P. Ball (2012b), Insights from the Jan Mayen system in the Norwegian–Greenland sea—II. Architecture of a microcontinent, *Geophys. J. Int.*, *191*, 413–435.

Pilidou, S., K. Priestley, E. Debayle, and O. Gudmundsson (2005), Rayleigh wave tomography in the North Atlantic: high resolution images of the Iceland, Azores and Eifel mantle plumes, *Lithos*, *79*, 453–474.

Poreda, R., J. G. Schilling, and H. Craig (1986), Helium and hydrogen isotopes in ocean-ridge basalts north and south of Iceland, *Earth Planet. Sci. Lett.*, *78*, 1–17.

Sallarès, V., P. Charvis, E. R. Flueh, and J. Bialas (2003), Seismic structure of Cocos and Malpelo Volcanic Ridges and implications for hot spot-ridge interaction, *J. Geophys. Res.*, *108*(B12), 2564, doi:10.1029/2003JB002431.

Sallarès, V., P. Charvis, E. R. Flueh, J. Bialas, and SALIERI Scientific Party (2005), Seismic structure of the Carnegie ridge and the nature of the Galápagos hotspot, *Geophys. J. Int.*, *161*, 763–788, doi:10.1111/j.1365-246X.2005.02592.x.

Schilling, J., M. Zajac, R. Evans, T. Johnston, W. White, J. Devine, and R. Kingsley (1983), Petrologic and geochemical variations along the Mid-Atlantic ridge from 29° N to 73° N, *Am. J. Sci.*, *283*, 510–586.

Sørnes, A., and T. Navrestad (1975), *Seismic survey of Jan Mayen*, Norsk Polarinst. Årbok, 37-52 pp., Norsk Polarinstitutt, Tromsø, Norway.

Talwani, M., and O. Eldholm (1977), Evolution of the Norwegian–Greenland Sea, *Geol. Soc. Am. Bull.*, *88*, 969–999.

Tan, P., J. Sippel, A. J. Breivik, M. Scheck-Wenderoth, and C. Meeßen (2016), Crustal and mantle structure of the greater Jan Mayen–East Greenland region (NE Atlantic) from combined 3D structural, S-wave velocity, and gravity modeling, *Eos Trans. AGU*, *97*(52), Fall Meet. Suppl., Abstract T43B-3034.

Thiede, J., and G. Hempel (1991), *Die Expedition ARKTIS-VII/1 mit FS "Polarstern" 1990*, Reports on Polar Research, vol. 80, 1–137 pp., Alfred Wegener Institute for Polar and Marine Research, Bremerhaven.

Trønnes, R. G., S. Planke, B. Sundvoll, and P. Imsland (1999), Recent volcanic rocks from Jan Mayen: Low-degree melt fractions of enriched northeast Atlantic mantle, *J. Geophys. Res.*, *104*(B4), 7153–7168, doi:10.1029/1999JB900007.

Trønnes, R. G., V. Debaille, M. Erambert, F. M. Stuart, and T. Waight (2013), Mixing and progressive melting of deep and shallow mantle sources in the NE Atlantic and Arctic, *Mineral. Mag.*, *77*, 2357.

U.S. Department of Commerce, National Oceanic and Atmospheric Administration, and National Geophysical Data Center (2006), 2-minute griddedglobal relief data (ETOPO2v2), http://www.ngdc.noaa.gov/mgg/fliers/01mgg04.html, Natl. Geophys. Data Cent., Boulder, Colo.

Vogt, P. R., G. L. Johnson, and L. Kristjansson (1980), Morphology and magnetic anomalies north of Iceland, *J. Geophys.*, *47*, 67–80.

Voss, M., and W. Jokat (2007), Continent-ocean transition and voluminous magmatic underplating derived from P-wave velocity of the East Greenland continental margin, *Geophys. J. Int.*, *170*, 580–604, doi:10.1111/j.1365-246X.2007.03438.x.

Voss, M., M. C. Schmidt-Aursch, and W. Jokat (2009), Variations in magmatic processes along the East Greenland volcanic margin, *Geophys. J. Int.*, *177*, 755–782.

Watts, A. B., and U. S. Ten Brink (1989), Crustal structure, flexure, and subsidence history of the Hawaiian Islands, *J. Geophys. Res.*, *94*, 10,473–10,500.

White, R. S. (1989), Initiation of the Iceland Plume and opening of the North Atlantic, in *Extensional Tectonics and Stratigraphy of the North Atlantic Margins*, vol. 46, edited by A. J. Tankard and H. R. Balkwill, pp. 149–154, AAPG Mem., Tulsa, Okla.

White, R. S., D. McKenzie, and K. O'Nions (1992), Oceanic crustal thickness from seismic measurements and rare earth element inversion, *J. Geophys. Res.*, *97*(B13), 19,683–19,715.

White, R. S., L. K. Smith, A. W. Roberts, P. A. F. Christie, N. J. Kusznir, and iSIMM Team (2008), Lower-crustal intrusion on the North Atlantic continental margin, *Nature*, *452*, 460–464, doi:10.1038/nature06687.

Wilkens, R. H., G. J. Fryer, and J. Karsten (1991), Evolution of porosity and seismic structure of upper oceanic crust: Importance of aspect ratios, *J. Geophys. Res.*, *96*(B11), 17,981–17,995.

Yaxley, G. M. (2000), Experimental study of the phase and melting relations of homogeneous basalt + peridotite mixtures and implications for the petrogenesis of flood basalts, *Contib. Mineral. Petr.*, *139*, 326–338.

Ye, S., J. P. Canales, R. Rihm, J. J. Danobeitia, and J. Gallart (1999), A crustal transect through the northern and northeastern part of the volcanic edifice of Gran Canaria, Canary Islands, *J. Geodyn.*, *28*, 3–26.

Yeo, I. A., N. Augustin, C. W. Devey, M. Deutschmann, L. J. Elkins, T. Laurila, K. Meisenhelder, E. Rivers, M. Rothenbeck, and F. M. van der Zwan (2012), The Northern Kolbeinsey Ridge, North Atlantic: Excess volcanism and ridge relocations close to Jan Mayen, *Eos Trans. AGU*, *93*(52), Fall Meet. Suppl., Abstract OS13B-1734.

Yeo, I. A., T. P. Lebas, N. Augustin, and A. Steinführer (2016), Segment-scale volcanic episodicity: Evidence from the North Kolbeinsey Ridge, Atlantic, *Earth Planet. Sci. Lett.*, *439*, 81–87.

Zelt, C. A., and R. M. Ellis (1988), Practical and efficient ray tracing in two-dimensional media for rapid traveltime and amplitude forward modelling, *Can. J. Explor. Geophys.*, *24*, 16–31.

Zelt, C. A., and R. B. Smith (1992), Seismic traveltime inversion for 2-D crustal velocity structure, *Geophys. J. Int.*, *108*, 16–34.